BNL-99516-2013-TECH
C-A/AP/369;BNL-99516-2013-IR

Energy Recovery Linac: HOM Absorbers

H. Hahn

January 2010

Collider Accelerator Department
Brookhaven National Laboratory

U.S. Department of Energy
USDOE Office of Science (SC)

DISCLAIMER

BNL-90923-2010-IR

C-A/AP/#369
January 2010

R&D ERL: HOM Absorbers

H. Hahn, I. Ben-Zvi, R. Calaga, L. Hammons, V.N. Litvinenko, W. Xu

Collider-Accelerator Department
Brookhaven National Laboratory
Upton, NY 11973

R&D ERL - HOM ABSORBERS

H. Hahn[#], I. Ben-Zvi, R. Calaga, L. Hammons, V. N. Litvinenko, W. Xu,

Brookhaven National Laboratory, Upton, NY 11973, USA

Abstract

Several future accelerator projects at the Relativistic Heavy Ion Collider (RHIC) are based on Energy Recovery Linacs (ERL) with high-charge high-current electron beams. Their stable operation mandates effective higher-order-mode (HOM) damping. The development of HOM dampers for these projects is pursued actively at this laboratory. A strong HOM damping was experimentally demonstrated both at room- and at superconducting- (SC) temperatures in a prototype R&D five-cell niobium SRF cavity with ferrite dampers. A novel type of ferrite damper over a ceramic break for a R&D SRF electron gun also was developed. For future SRF linacs longer cryomodules comprising of multiple superconducting cavities with reasonably short transitions between them are planned. In such a configuration, the dampers, located closer to the cavities, will be at cryogenic temperatures; this will impose additional constraints and complications. Two room-temperature mock-up five-cell copper cavities were used to study various damper configurations. This paper presents results of simulations and measurements for several configurations.

I. INTRODUCTION

The Collider-Accelerator Department at BNL is actively working on various accelerator projects based on high current SRF ERLs: (1) an R&D Energy Recovery Linac (ERL) facility [1]; (2) electron-ion collider eRHIC and its first stage, MeRHIC [2]; and (3) coherent electron cooling [3]. The requirements for high-current, high-brightness, and high-charge in these projects do require development of effective higher-order-mode (HOM) dampers.

The R&D ERL facility is designed to operate with a high-current, up to 0.5 A or with high-charge bunches up to 5 nC. It is based on a five-cell SC Linac and a half-cell SC photo-injector RF electron gun [4], both operating at a frequency of 703.75 MHz. With a highly flexible lattice of the electron beam return loop, the R&D ERL will serve as a test bed for the technologies and concepts necessary for future high current ERL-based projects.

The SC 5-cell cavity has a very long and large diameter vacuum pipe which connects to the room temperature HOM dampers that are installed outside of the cryostat. These HOM dampers use ferrite absorbers. Results of the studies of the HOM damping at room-temperature with these ferrite absorbers has been published previously [5]. Since then, several cold tests have been performed. In this paper, the high-Q induced changes in these measurements are presented.

The eRHIC electron accelerator will use SRF linacs based on five-cell SC cavities with highly damped HOMs, similar to that used for R&D ERL [6]. The cost of the SRF linacs and their real-estate gradients are the key consideration in this project. The eRHIC-type SRF cryomodules should be also compact and modular. Having gained the

experience with ferrite dampers at R&D ERL, various alternatives including capacitive HOM dampers are also explored.

This paper is organized as follows. Section II summarizes the results from the cold ERL measurements, and gives a table of HOM shunt impedances for use in beam-breakup studies. In Section III, issues related to a modular design of future SRF linacs are addressed. The measurements of HOM damping achieved with capacitive probes placed between two 5-cell copper cavities, are presented in Section IV. Section V reports on the same measurements performed with a ferrite absorber. Finally, Section VI is dedicated to describing a novel damper configuration with a ferrite absorber placed over a ceramic vacuum chamber, constructed for the SRF electron gun. This design can be used in an eRHIC type cryomodule, where a cold ceramic vacuum break may allow using ferrite absorber at higher temperatures.

II. THE R&D ENERGY RECOVERY LINAC

The HOMs in the Brookhaven R&D ERL are damped with room-temperature ferrite dampers located outside the cryostat and at both ends of the cavity's vacuum vessel, as seen in Fig. 1. The ferrite properties and cavity measurements at room temperature were reported previously [5]. The assembled 5-cell cavity cryostat underwent several cool-down sessions to 4 K- and 2 K-temperatures providing the HOM data for this paper, wherein the measured results are analyzed via the CST Microwave Studio (MWS) program. The HOM structure and parameters are established by the basic shape of the cavity, but are modified by the large aperture, 24 cm dia., and the asymmetric lengths, 55- and 52.5-cm long, of the beam-tube sections connecting the ferrite dampers to the cavity, as detailed in Fig. 2.

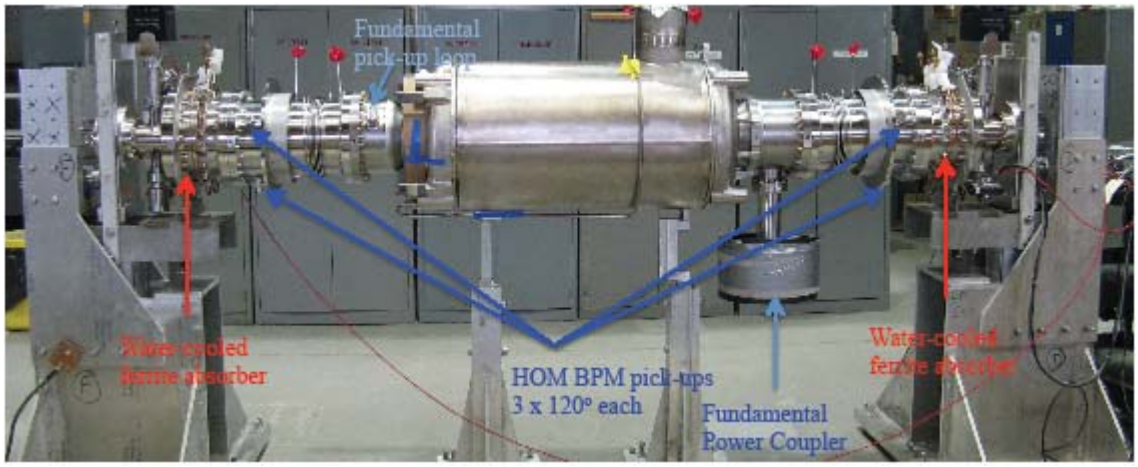

FIG. 1: View of R&D ERL 5-cell cavity vacuum string assembly with ferrite dampers and pick-up electrodes, but without its cryostat

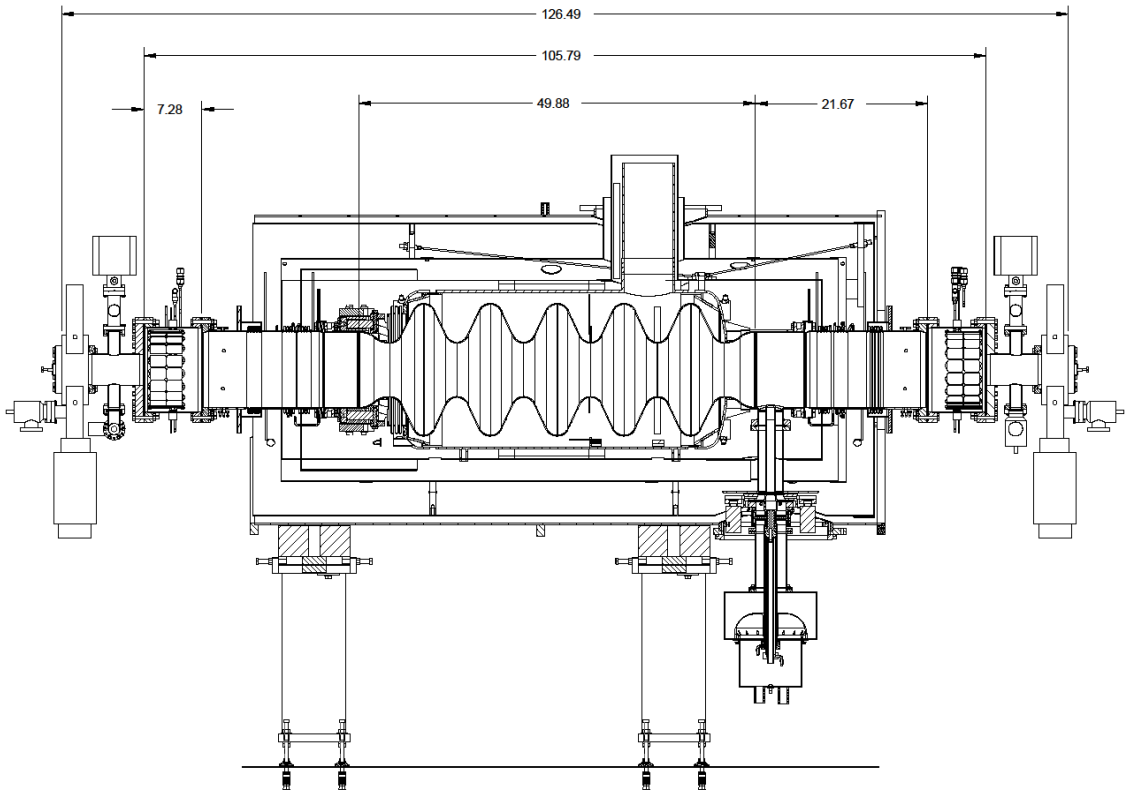

FIG. 2: The cross-section of the R&D ERL 5-cell cavity vacuum string assembly (dimensions are given in inches)

Measurement Data.

As shown in Fig. 1, two sets of the pick-up electrodes, located at each side of the cavity vacuum string, are intended as beam position monitors (BPMs) for centering the beam during operation. At the same time, they are available to collect the cavity's HOM data. Each of these sets has three pick-up probes spread evenly around the circumference 120-degrees apart, and in the text are referred to as the 2-, 6-, and 10-o'clock BPM pick-up probes. In addition, depending on the operational mode, there was limited access to the RF cavity pick-up probe, and to the fundamental power coupler.

The frequencies and *Q*-values of the cavity string with the HOM were obtained for this paper from forward scattering coefficient (S21) measurements between the bottom "6 o'clock" pick-up probes located at opposite sides of the cavity. To study the beam tubes' resonances, the two pick-up probes from the same set at "2 and 10 o'clock" were employed.

Fig. 3 shows the HOM spectrum in the first pair of dipole pass-bands with the cavity at room temperature. The proper cavity resonances are identified as peaks in the through measurement (BPM 6 6), and as dips in the local BPM measurement (BPM 2 10). The additional beam-tube resonances at ~780 MHz (a dipole mode), and at ~890 MHz (a monopole mode) are visible in the local measurements. Fig. 4 is an expanded plot of the unexpected resonances in the beam tube below the cutoff frequency. The field patterns for two modes simulated by MWS are shown in Fig. 5. The S21 structure of the

downstream pipe, housing the fundamental power coupler (FPC), has notches characteristic of reflections caused by the long waveguide connected to the FPC.

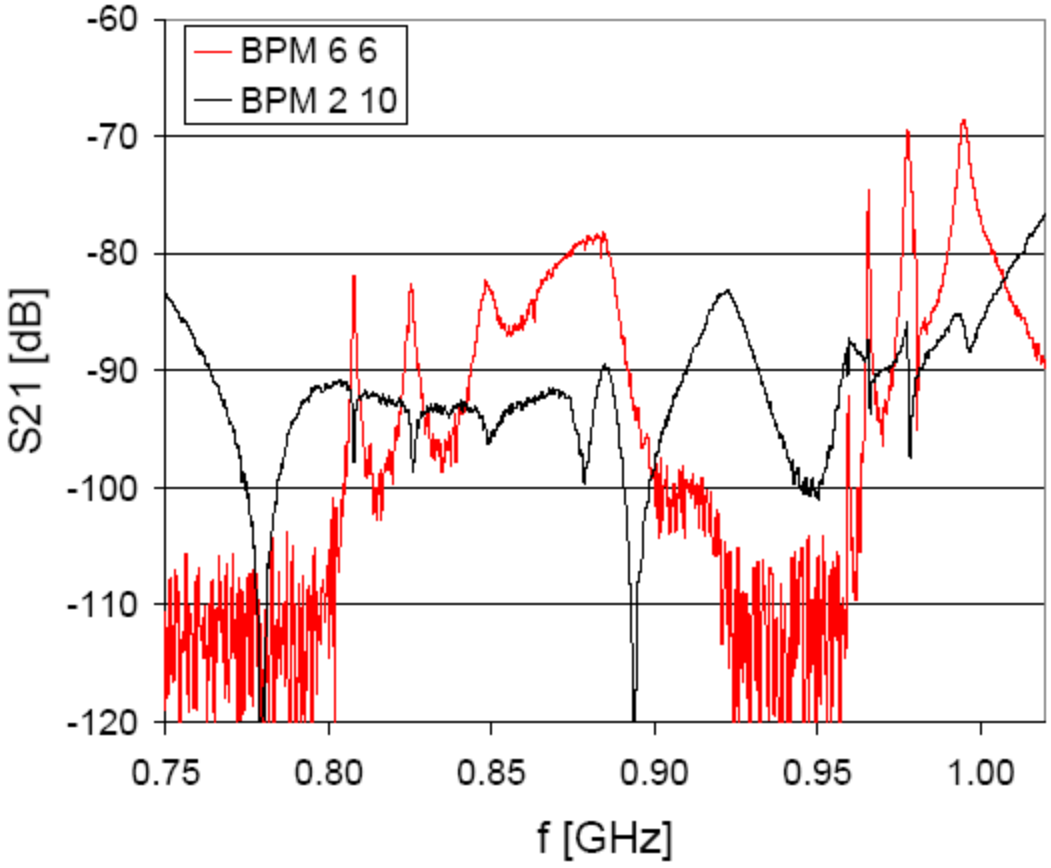

FIG. 3: HOM spectra of the R&D ERL cavity at room temperature. Red curve shows the transmission through the cavity (BPM 6 6), while the black curve shows transmission between two probes in the upstream tube (BPM 2 10).

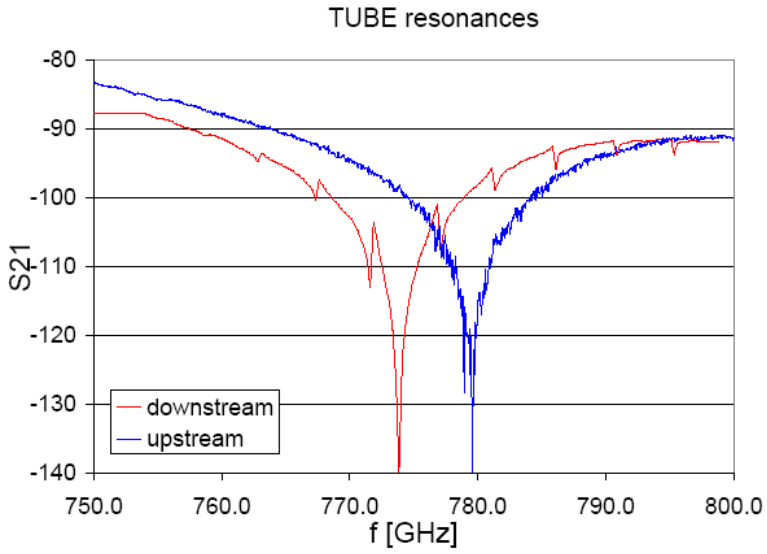

FIG. 4: Resonances in the upstream- (blue) and downstream-(red) beam tube. The latter houses the fundamental power coupler (FPC). Its additional resonant structure is caused by the FPC's waveguide.

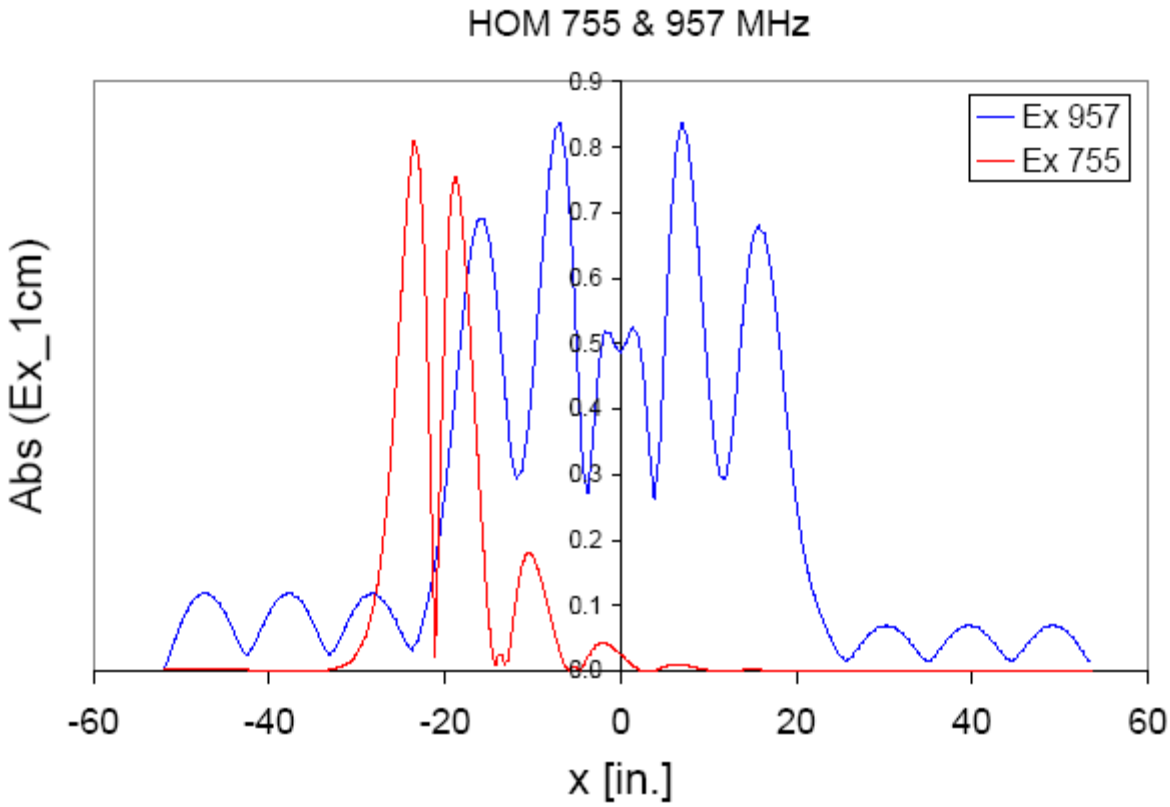

FIG. 5: Plots of the longitudinal electric field component at 1 cm off-axis for a beam tube-mode (red), and for a quasi-trapped mode (blue)

Fig. 6 compares the S21 spectra of the 5-cell cavity for normal-conducting- (NC) and superconducting-(SC) states in two pass-bands. Most NC measurements were performed after the SC tests during warming before reaching room temperature. A small increase of the Q-values between these states, for the majority of the modes, clearly indicates that the ferrite absorbers provide good HOM damping. Only the semi-trapped 960 MHz mode is weakly coupled to the ferrite absorbers (see Fig. 5) and has a relatively high Q ~ 50,000. Fig. 7 shows detailed studies of this mode at room temperature, at 4 K, and at 2 K.

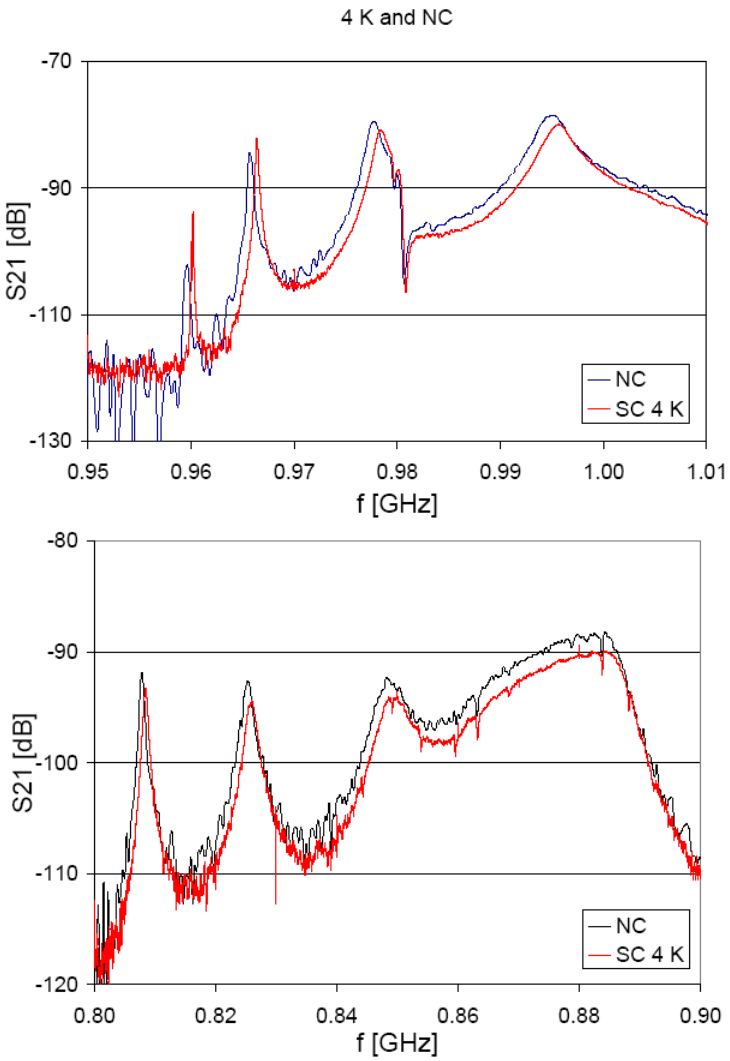

FIG. 6. Spectra of HOMs in the ERL 5-cell cavity in the normal- (NC) and in the superconducting-state (at 4 K).

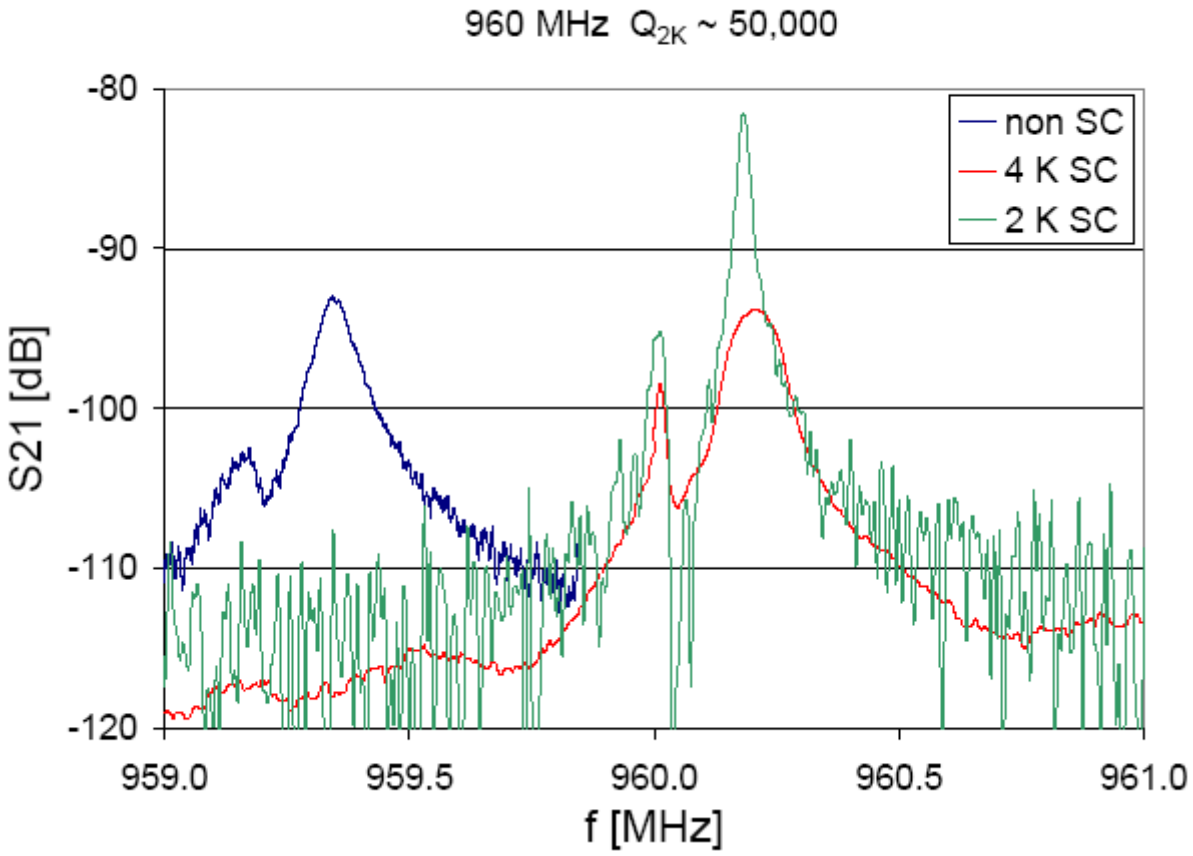

FIG. 7: Resonance curves of the quasi-trapped ~960 MHz mode at different temperatures.

Data analysis and simulation results.

Measurements of the cavity provide the HOM frequencies and *Q*-values, but fall short of providing the impedances, i.e., the R/Q. The R/Q values are important for simulating the transverse break-up instability threshold of the beam. Thus, the shunt impedances must be obtained through MWS simulations. A picture of the cavity model used in these simulations is shown in Fig. 8. It was assumed that achieving a 10^{-4} relative accuracy for HOM frequencies would be sufficient. However, the difference between the simulated- and measured-frequencies was significantly larger than this goal. The difference is attributed to large changes in temperatures, pressure-induced geometry, and the lack of a detailed 3D model for the FPC and the pick-up probe's structures.

In general, simulations of the cavity in the presence of ferrite material are time consuming. Initially, the HOM frequencies in the two pass bands were simulated for a copper cavity without ferrite. Later, the study focused on individual resonances with ferrite absorbers, using $\varepsilon = 13$ and $\mu = 4(1 - j2.5)$ at 1 GHz for their properties. The simulation runs for critical modes were performed in the JDM eigenvalue solver with settings of 8-, 16-, and 0.1-lines per wavelength. This calculation produced the lowest mesh size, ~ 200,000 mesh points, of which about 2/3 were located in the ferrite

absorbers. Runs with ~100,000 mesh points gave a 10^{-3} accuracy in the HOM frequencies, and ~10% in R/Q accuracy.

Table I summarizes the results of the measurements and the simulations for dipole modes in the 0.75-1 GHz band. The resonance frequencies, labeled f_{Data}, are measured with the network analyzer as shown in Fig. 3. The MWS simulation results for the dipole R/Q is obtained from the longitudinal electric field integral done off-axis at $a = 1$ cm and interpreted as

$$\left(R/Q\right)_{\perp} = \left(R/Q\right)_{1\mathrm{cm}} / ka^2$$

with $k = \omega / c$. In several cases, the MWS model underestimates the strengths of the ferrite damping and overestimates the Q-values compared with the measurements, possibly due to the loss assumed for the ferrite. The shunt impedance R is obtained using simulated R/Q multiplied either by the measured $Q_{2\mathrm{K}}$ (when available) or by the MWS Q.

The lowest frequency (0.75-0.9 GHz) pass band essentially is comprised of TE_{11} modes that couple strongly to the ferrite absorber and, consequently, have low Q-values. The number of the 10 modes found in the simulation with the same polarization exceeds the expected 5 cavity resonances. The additional modes are either beam-tube modes, end-cell modes, or longitudinally asymmetric cavity modes. The second pass band (0.95-1.0 GHz) is comprised of TM11 modes with weaker coupling to the ferrite absorbers, and correspondingly higher Q-values. The quasi-trapped mode at ~960 MHz is a typical example of this trend.

Some predicted resonances were not found in the measurements. Furthermore, the measured Q-values of some modes differ significantly from the predicted values. Probable explanations for these discrepancies are (a) weak coupling of the pick-up probes with strongly asymmetric modes, and (b) lowering of Qs due to apparent broadening of the rotated split modes. The transverse beam break up (TBBU) simulation for the ERLs will be based on the worst case scenario with the simulated shunt impedances or on higher SC data, if available. Preliminary BBU studies show that few HOMs, mostly the proper cavity dipole modes at 966 and 978 MHz, are the main players in the TBBU [7].

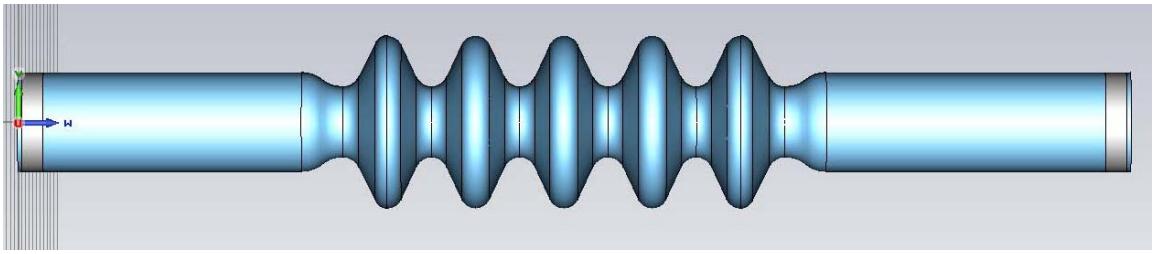

FIG. 8: Model of R&D ERL 5-cell cavity used for MWS simulation

Table I. Dipole modes in the R&D ERL cavity.

Data			MWS wo FRT		MWS				
f_{Data} [MHz]	Q_{NC}	$Q_{2\text{K}}$	f [MHz]	R/Q_{1cm} [Ω]	f [MHz]	Q	R/Q_{1cm} [Ω]	R/Q [Ω/m]	$R_{\perp}$ [kΩ/m]
774			752.3	0.003	752.2	382	0.0007	0.42	0.2
780			755.1	0.004	754.9	322	0.0083	5.23	1.7
			806.1	0.002	804.9	586	0.0032	1.93	1.1
808	911	~900	810.9	0.010	809.6	180	0.0217	12.81	11.7
			818.5	0.033	817.3	155	0.0220	12.87	2.0
825	390	~390	830.1	0.009	828.5	335	0.0073	4.19	1.6
849	147	?	852.5	0.431	851.2	605	0.3931	220.54	133.4
			875.3	1.799	874.9	433.2	1.6441	897.38	388.7
883			890.8	1.438	889.1	176	1.3370	718.15	126.4
			897.7	0.730	896.2	215	0.7683	409.40	88.0
			929.6	0.374	927	113	0.2606	134.25	15.2
			944.5	0.220	941.2	86	0.3229	163.83	14.1
960	12,550	50,000	958.1	0.002	957.4	40950	0.0016	0.81	40.5
966	3850	5,400	964.4	0.105	963.6	6683	0.1073	53.18	355.4
978	800	~800	976.4	0.319	975.6	2288	0.3212	157.24	359.8
995	315	~320	993.2	0.098	990.2	1735	0.0974	46.99	81.5
					1019	67	0.0204	9.56	0.6

III. CAVITY STRING MODEL

The proposed eRHIC machine will consist of an electron linac employing SC cavities of the type being used in the ERL facility, but upgraded following the experience gained in developing this cavity [6]. A key consideration for the design changes is the need for highly compact, modular cryomodules and accompanying structures. The present concept views the electron linac as a chain of sections (Fig. 9), each employing six five-cell cavity cryo-modules. The HOM dampers will be placed into the cold section between two cavities. Having gained the experience with ferrite dampers, the primary focus in the present study is to explore alternative HOM dampers.

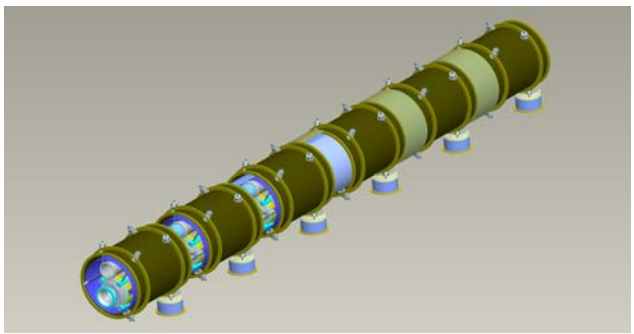

FIG. 9: A MeRHIC linac section with 6 cavity cryo-modules

Replacing ferrite with capacitive probes is one option for longitudinal space savings in a chain. However, a chain of cavities presents problems not encountered in a single cavity, notably possible coupling of HOMs and even of the fundamental in neighboring cavities. The availability of two five-cell copper cavities provides an opportunity for exploratory damper measurements applicable to the chain, which is sufficiently replicated by the two-cavity arrangement in Fig. 10.

FIG. 10 : The HOM damper ring with capacitive probes between two copper cavities

Estimates for the R/Q of dipole HOMs in a chain beyond those for the Brookhaven R&D ERL Cavity (locally known as Experimental Cavity, ECX-BNL I) in Table I will depend on the new cavity's (BNL II) design and the geometry and length of the interconnecting beam tube. The parameter range was explored via the two Microwave Studio (MWS) models in Fig.11, representing the ECX-BNL I cavity with symmetric beam tubes added, and the planned BNL II cavity [6].

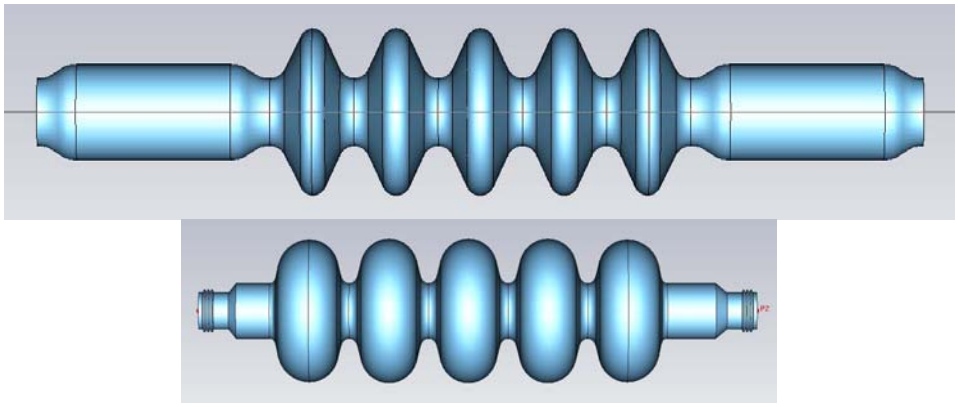

FIG. 11: MWS models for the ECX (BNL1) (top) and the planned BNL2 cavities (bottom) [6]

Two important questions concern the impact of asymmetry and of losses on the cavity shunt impedance via the R/Q and Q values. The ERL facility was configured with beam tubes of uneven length, so producing longitudinal mode splitting, with 806/ 811 MHz the example for the lossless cavity, and 805/810 MHz for the damped one. In the ERL, the R/Q values for the proper cavity modes in lossless- and damped-modes agree within 10% and are qualitatively equal in the split cavity and end-cell modes. Accordingly, the search for R/Q can be done with a lossless model for the damper-equipped cavity. The question about asymmetry and beam tube length remains to be answered.

Impedance projections for the eRHIC cavity are produced in Fig.11 with the MWS simulations for the two models. The results of the MWS simulations for the R/Q of the two lowest dipole pass bands are given in Table 2 for the two cavity examples, the ECX cavity with the attached symmetric beam tubes of lambda (42.6 cm) length, and the BNL2 cavity without short tubes. The 10 cm diameter waist in BNL2 essentially decouples neighboring cavities. All simulations were done with the cavity ends shorted to avoid radiation damping from open ends confusing the data. Again, the larger number of resonances actually found in the ECX cavity compared to the expected ones in a free-standing single cavity, identified as "C" in the table. The additional resonances are pure beam-tube resonances, B", or are located mainly in the end cells, "E".

Table 2: Simulated R/Q of dipole resonances in free-standing single cavity. Proper cavity modes are identified as "C", beam tube and end cell resonances as "B" and "E"

BNL 1 with tubes				BNL II			
f [MHz]	R/Q_{1cm} [Ω]	$R/Q_{\perp}$ [Ω/m]	Mode Type	f [MHz]	R/Q_{1cm} [Ω]	$R/Q_{\perp}$ [Ω/m]	Mode Type
775.69	0.003503	2.16	B				
775.71	0.005878	3.62	B				
808.82	0.003477	2.05	C	817.36	0.0137	8.0	C
826.17	0.02781	16.08	C	832.94	0.0728	41.8	C
849.08	0.1748	98.31	C	856.59	0.5320	296.6	C
870.13	1.2041	660.85	C				
883.26	1.7304	935.58	C	892.18	2.3037	1233.1	C
890.06	0.9097	488.09	C				
931.04	0.8552	438.65	E				
931.06	0.2273	116.59	E				
959.43	0.001826	0.91	C	934.78	1.1619	593.6	C
965.68	0.1062	52.52	C	947.08	0.0028	1.4	C
977.63	0.3045	148.74	C	986.00	0.6876	333.0	C
994.38	0.09844	47.28	C	997.60	1.1445	547.9	C
1064.83	0.008471	3.80	B	1002.89	0.1958	93.2	E
1065.73	0.05258	23.56	B	1003.50	0.2227	106.0	E
1199.06	0.03856	15.36	E				

The ERL design was based on the concept that a large beam-tube aperture, here 24 cm, allows exit of the HOMs from the cavity to the damper, a fact that was confirmed by the various measurements. However, the large diameter of the beam tube diameter allows the generation of beam-tube resonances, with Fig. 12 as an example, which are strongly damped by being locally connected to the dampers. In contrast, the end-cell modes, as in Fig. 13, may not be strongly coupled to the dampers and less damped.

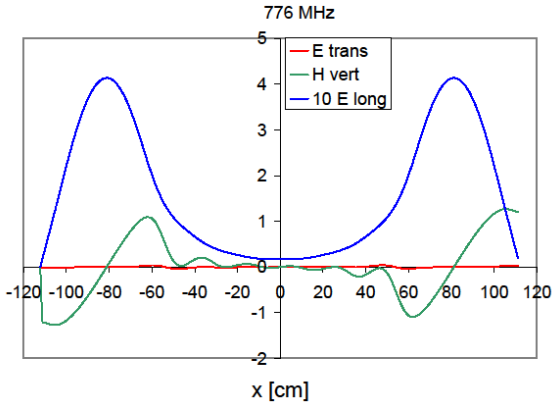

FIG. 12: Fields in beam tube at 776 MHz

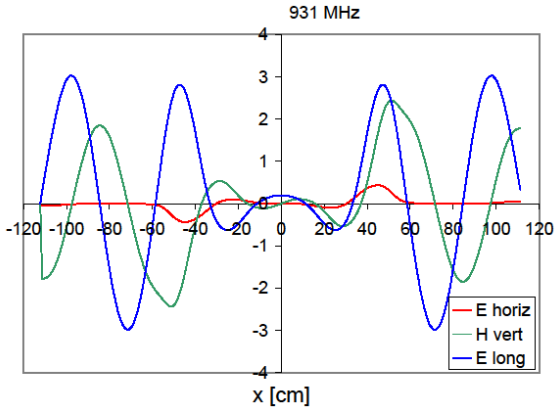

FIG. 13 : Fields in the end cell at 931 MHz

A further design concern stems from the possible existence of trapped modes that are uncoupled to the damper. Thus, BNL1 at 959 MHz is a prototypical example of a quasi-trapped "proper" cavity mode whose fields are concentrated in the center cell with minimal coupling to any damper in the adjacent beam tube. The longitudinal- and transverse-electric field components, and the transverse magnetic field components shown in Fig. 14 are concentrated within the nominal cavity length of 2 × 63 cm (~2 × 25 in.). Only weak tails of these fields extend outside the cavity towards the dampers.

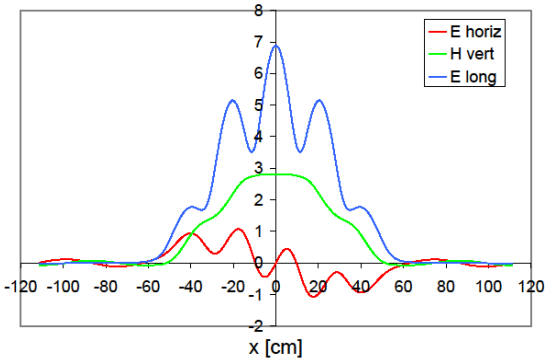

FIG. 14 : Fields of a quasi-trapped mode in the cavity at 959 MHz

The simulated results for the ECX cavity suggest that good R/Q estimates of a cavity can be obtained from simulation independently of the damping losses. This conclusion holds even in the presence of ferrite-induced field changes. The effect of losses on the field shape is resolved by comparing the simulations in Fig. 5 and Fig.14. The plots in Fig. 14 were obtained for a lossless structure, but qualitatively agree with those from the ferrite-damped ECX cavity (Fig. 5). In the latter, the quasi-trapped mode at ~960 MHz also has no fields or minimal ones extending from the cavity. However, the peak field in the center cell is strongly altered by the losses and, to a smaller degree, by the length of the attached beam tubes. In contrast, the beam-tube mode at ~770 MHz is restricted to the beam tube on one cavity end.

Another effect of large beam tubes is the coupling resulting in a frequency shift and splitting of the HOMs in neighboring cavities. This is clearly seen in the HOM spectrum of un-damped Cu cavities, shown in Fig. 15. Depending on the inserted beam-tube length between cavities, coupling even at the fundamental mode frequency must be considered. The tubes' length, including the damper ring between the Cu cavities in Fig. 10, is sufficient to decouple the fundamental. The waist in BNL2 minimizes or removes the HOM coupling.

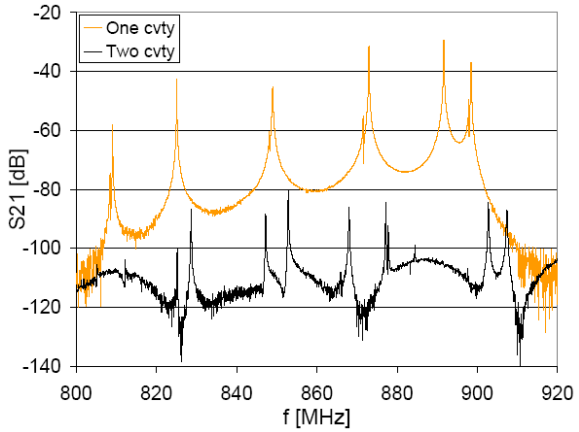

FIG.: 15. Frequency splitting of HOMs in the combined Cu cavities.

A major concern in designing HOM dampers is to minimize the associated fundamental mode losses. In the ERL, this was achieved by placing the ferrite damper sufficiently far away from the cavity proper. Such a solution is not appropriate for a space-constrained string. Assuming individual excitation of cavities softens the constraint on the cavity spacing, placing the center of end cells apart by $(2n+1)\,\lambda/2 \approx 60$ cm provides a field minimum at the beam tubes' center and minimizing the fundamental mode coupling to the dampers [8].

IV. CAPACITIVE HOM DAMPERS

Alternate methods of HOM damping use capacitive probes and inductive loops. Due to their simple construction, capacitive probes have been studied as dampers in copper cavities. In contrast to ferrite dampers, the capacitive probes would be attached to a spacer ring and placed in the cold section between two cavities. Fig. 16 and Fig.17 show the ring with four capacitive "mushroom" probes, each with a 2- inch diameter disk on a

1-inch-long stem. The four capacitive probes are centered in the ring and are placed 7 inches from the left cavity, and 8.5 inches from the right cavity. The S21 transfer coefficient is measured between two Fundamental Power Couplers, FPC1 and FPC2 shown in Fig. 10, thus yielding data for the left cavity.

FIG. 16: Connecting tube with damper ring

The frequencies and measured *Q*-values of the left cavity in this set-up are listed in Table 3, where the simulated frequencies for one single cavity are added as guidance. In a SC cavity, the *Q*-external practically equals the loaded *Q* for the determination of the shunt impedance. The Q-external is obtained from the unloaded Q_0 and loaded Q_L as

$$Q_X = \frac{Q_L Q_0}{Q_L - Q_0}$$

The column indicated by (Q_X (wo)) obtained with probes of equal stem length but without disks, points to the 2-inch dia., 1-inch-long capacitive probes as being the appropriate dampers. Expectedly, placing damper rings at the ends of both cavities will halve the *Q*-values.

The fields of the HOMs in the beam tube are stationary, even though they are above cutoff, and the axial location of the probes determines the coupling strength. A damper of finite axial length has a better chance of missing a node and of connecting to the mode. As a finite-length approximation, measurements with staggered placements of the four probes were performed and the results, listed in Table 4, indicate improved damping. By extrapolation, staggered dampers with three probes per ring at 2, 6, and 10 o'clock, or at 4, 8, and 12 o'clock seem optimum.

Table 3 : Simulated and measured frequencies and measured Q-values
Q_X (wo) is for probes with equal length but without disk

f_{MWS} [MHz]	f_{Data} [MHz]	Q_0	Q_L	Q_X	Q_X (wo)
808.8	806.3	11,370	9940	79,033	311,822
	814.3	7090	5310	21,151	125,194
826.2	825.1	17,050	4190	5555	42,889
	828.6	9450	2490	3381	24,249
849.1	847.1	1,440	3610	4936	44,270
	852.8	10,980	1680	1983	17,521
870.1	867.9	10,520	2770	3760	35,593
883.3	877.2	13,570	2603	3221	38,448
890.1	884.3	7990	3290	5593	50,046
959.4	958.2	35,390	29,460	175,816	4,283,410
	958.7	34,900	2,880	138,606	5,501,509
965.7	965.6	13,950	17,760	65,027	26,151
977.6	976.7	19,370	3440	4183	124,384
	978.0	23,400	13,000	29,250	165,414
994.4	994.5	1340	1100	1199	8335
	996.8	15,090	4840	7125	71,821

Table 4 : Frequencies and Q-values with staggered dampers

f_{Data} [MHz]	Q_0	Q_L	Q_X
808.0	5810	3260	7428
808.6	4260	2520	6170
819.3	5660	4460	21,036
825.0	17,920	100	101
833.0	9740	4970	10,148
846.2	12,440	1540	1758
854.6	11,310	3280	4620
865.8	3420	10	10
877.0	12,180	1400	1582
883.2	6300	2040	3017
958.7	33,040	22,790	73,462
965.5	28,650	4830	2809
976.9	13,050	100	101
877.8	15,670	1850	2098
995.0	8660	3880	7029
996.4	8770	2240	3008

FIG. 17: Damper ring with four "mushroom" capacitive probes

Since the damper ring with its probes is located between the FPC and RF pickup (PU) probe, cross coupling at the fundamental of probe to FPC and PU must be considered, in addition to HOM damping. The length of the damper ring and its location with respect to the cavities is a critical design parameter, and must be selected for strong damping, together with the shortest overall length and minimum coupling to the fundamental. The *Q*-external at the fundamental mode attributable to each of the four probes in the ring and its variation with their geometry and location was measured and is shown in Fig. 18.

The HOM damping in Table 3 is achieved with an external cavity *Q* of a low $\sim 1\times10^{8}$; higher values are limited by the required damping. The capacitive ring adds 5 inches to the cavity's length. An order-of-magnitude reduction of the fundamental load would require adding about 3 inches to the length of the beam tube. Fundamental cross coupling between the FPC to a single damper was $S_{21}\sim3\times10^{-3}$, which complicates the thermal design of the fundamental filter.

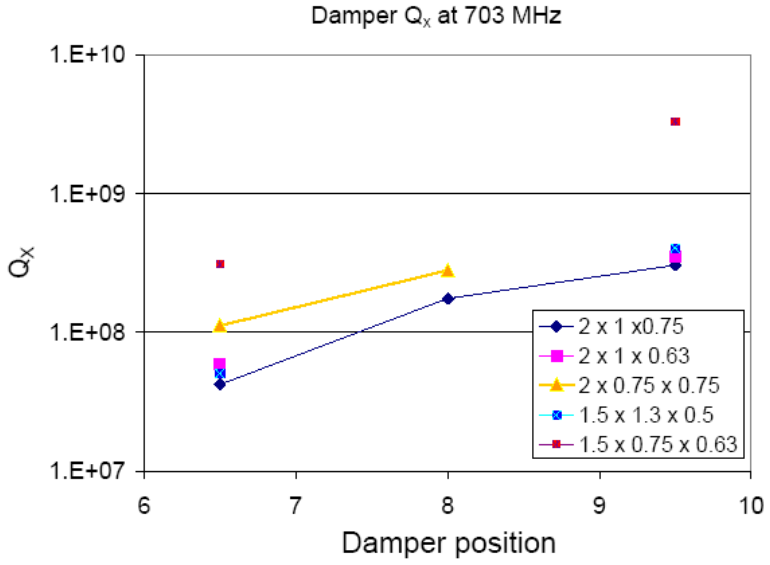

FIG. 18: Q-external versus damper position and probe size (disk diameter × stem length × stem diameter in inches)

Reduction of fundamental losses requires adding to the length of the beam tube or incorporating a filter, possibly of the type illustrated in Fig. 19. The filter shown was designed by Sekutowicz for a prototype electron-gun cavity [9], but the separation

between the fundamental frequency and the HOM high-pass is not steep enough, and a different filter would have to be developed.

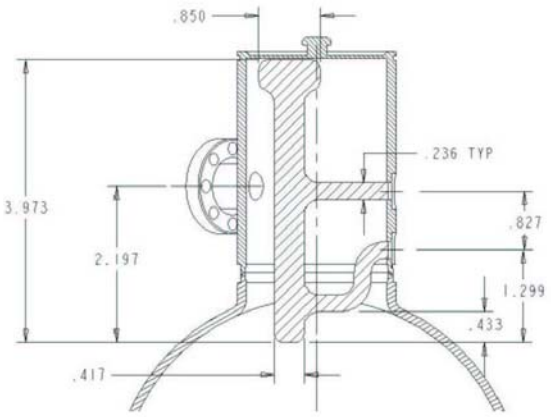

FIG. 19: HOM damper with built in fundamental filter (dimensions in inches)

V. FERRITE DAMPERS

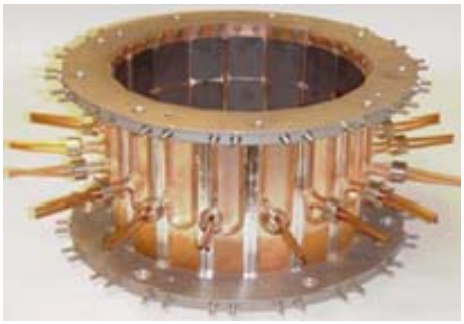

FIG. 20: Prototype HOM ferrite damper

A photograph of the prototype ferrite absorber is shown in Fig. 20. This absorber was placed between the 5-cell copper cavities, Fig. 21, and used this configuration for comparison with the capacitive ring damper (see previous section). The free ends of the 5-cell cavities were shorted by Cu plates to eliminate any radiation or coupling with the outside environment. The set-up for the S21 measurement between the FPCs at the cavities was similar to that for the capacitive probe. Fig. 22 compares the S21 plots for an un-damped and ferrite-damped 2-cavity string.

FIG. 21 : Ferrite HOM damper installed between the 5-cell Cu cavities

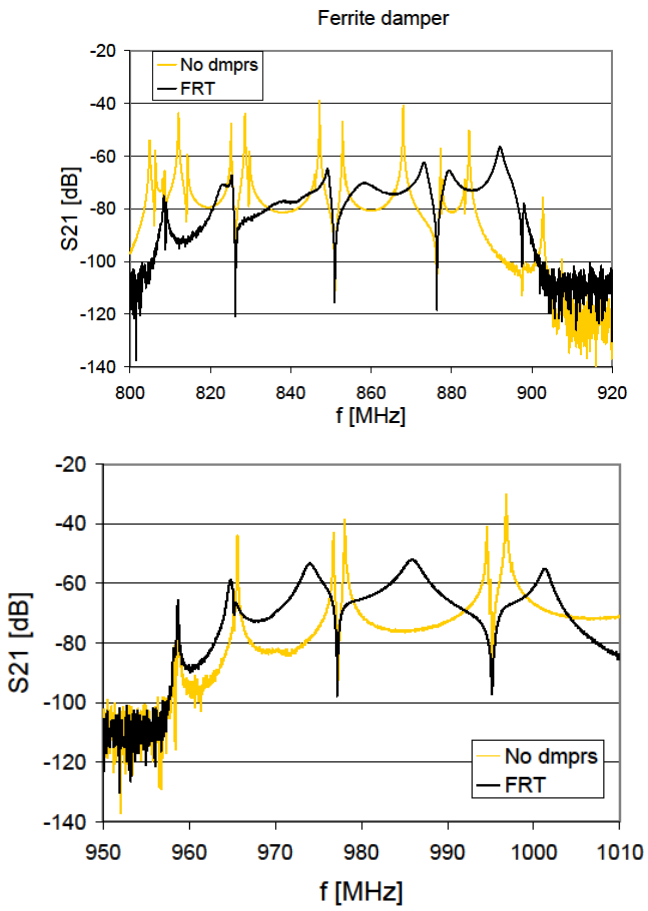

FIG. 22: S21 for 2-cavity string with (black line) and without (yellow line) ferrite damper

The ferrite damper provided the strongest HOM damping compared with that by the capacitive dampers described in the previous sections. Table 5 shows measured parameters for the HOMs. Some Q-values are significantly lower than those measured with the single R&D ERL 5-cell cavity (see Section II). One source of additional damping is radiation coupling into the unexcited cavity. An other possible explanation for this is that the ferrite damper is much closer to the cavity in the test set-up compared with that in the R&D ERL case.

Table 5 : Parameters of ferrite-damped HOMs for the two-cavity string

f [MHz]	Q_L	f [MHz]	Q_L
1st pass band		2nd pass band	
808.4	4690	958.1	13,210
809.0	4380	958.6	13,390
825.3	1480	964.7	1950
849.1	910	974.0	580
858.2	130	985.9	460
873.1	580	1001.3	790
879.3	410		
892.0	630		
897.9	2110		

VI. FERRITE DAMPER USING CERAMIC BREAK

Attaining high real-estate gradients may preclude increasing the length of the vacuum pipe between the cavities to allow the decay of the evanescent fundamental wave to a negligible level at the damper. In this case, the ferrite can absorb some measurable portion of the fundamental RF power in addition to significant HOM power. It is impossible to make the numerous transitions to and from room temperature to accommodate room-temperature ferrite absorbers.

As a solution, a novel damper with ferrite absorber located outside the ceramic vacuum tube is proposed. Such a configuration has multiple advantages. First, it moves the brittle ferrite material outside the particulate-free SRF-class vacuum, and second, it simplifies cooling and may allow the ferrite damper to be placed outside the cryogenic line. The ceramic can serve as an effective thermal transition that may be useful in various applications.

Fig. 23 is a drawing of such an absorber developed for the R&D ERL SRF gun [4]. The ceramic (alumina) vacuum tube with 10-cm internal diameter is coated with a thin film of titanium-enhanced stainless-steel (with an end-to-end resistance of ~ 100 MΩ) to prevent static charge accumulation. The ferrite tiles, located outside the tube in the atmosphere, will be cooled by simple means. The design of a "clamshell" structure that holds the ferrite tiles in place allows other damping materials to be quickly and easily installed and tested. This is particularly useful because the ceramic can protect superconducting components from the dust or chips that might result from damage to the ferrite tiles that serve as the HOM-damping material. The multi-layer structure of such an absorber was analyzed, and proved that the damping properties of such a system remain acceptable [10]. The prototype of such an absorber was fabricated and will be used to verify predictions.

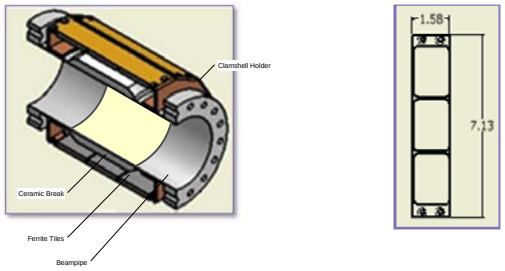

a b

FIG. 23: (a) Ferrite HOM damper with 10 cm i.d. ceramic break. (b) Detail of plate with ferrite tiles. The plates are held in place by the clamshell holder indicated in (a). Dimensions are in inches.

ACKNOWLEDGEMENTS

The authors thank Dr. D. Lowenstein for his advice and comments on the manuscript. This work was supported by Brookhaven Science Associates, LLC under Contract No. DE-AC02-98CH10886 with the U.S. DOE.

References

[1] I. Ben-Zvi, FR101 in Proc. 13th international Workshop on RF Superconductivity, Beijing, China, (2007), and *ERL Prototype at BNL*, Abstract in Proc. RF Superconductivity 2009, Berlin, Germany, p.41.

[2] V. Ptitsyn, J. Beebe-Wang, I. Ben-Zvi, A. Burrill, R. Calaga, X. Chang, A. Fedotov, H. Hahn, Y. Hao, L. Hammons, D. Kayran, V. N. Litvinenko, G. Mahler, C. Montag, B. Parker, E. Pozdeyev, T. Roser, A. Pendzick, S. Plate, S. Tepikian, D. Trbojevic, N. Tsoupas, J. Tuozzolo, G. Wang, E. Tsentalovich, *MeRHIC - Staging Approach to eRHIC,* Proc. 2009 Particle Accelerator Conference, Vancouver, Canada.

[3] V. N. Litvinenko and Y. S. Derbenev, Phys. Rev. Letters **102** (11) (2009).

[4] R. Calaga, I. Ben-Zvi, M. Blaskiewicz, X. Chang, D. Kayran, and V. Litvinenko, Physica C-**441** (1-2), 159-172 (2006).

[5] H. Hahn, E. M. Choi, and L. Hammons, Phys. Rev. S T. Accel. Beams, **12,** 021002 (2009).

[6] R. Calaga, Proc. SRF2009 Conference, Berlin, Germany, p. 514, and http://cern.ch/rcalaga/704MHz, (private communication)

[7] J. Kewisch, (private communication)

[8] V. N. Litvinenko, (private communication)

[9] Y Zhao and H. Hahn, *HOM measurement and simulation*, Internal Report C-A/AP/161 (BNL, 2004)

[10] L. Hammons and H. Hahn, *HOM Absorber development for SC BNL ERL*, Proc. Cornell ERL09

[11] H. Hahn, *Matrix solution to longitudinal impedance of multi-layer circular structures*, Internal Report C-A/AP/336 (BNL, 2008)